Proceedings of ASME Turbo Expo 2011
GT2011
June 6-10, 2011, Vancouver, British Columbia, Canada

GT2011-45899

INFLUENCE OF COOLANT FLOW RATE ON AERO-THERMAL PERFORMANCE OF A ROTOR BLADE CASCADE WITH ENDWALL FILM COOLING

G. Barigozzi, F. Fontaneto, G. Franchini, A. Perdichizzi
Università degli Studi di Bergamo Dipartimento di Ingegneria Industriale
Viale Marconi 24044 Dalmine (BG) Italy Tel +39 0352052306 fax +39 035562779
giovanna.barigozzi@unibg.it, fabrizio.fontaneto@unibg.it, giuseppe.franchini@unibg.it,
antonio.perdichizzi@unibg.it

M. Maritano, R. Abram
Ansaldo Energia S.p.A. - Hot Gas Path Engineering
Via N. Lorenzi 8 - 16152 Genova Italy Tel +39 0106557209
maritano@aen.ansaldo.it, abram@aen.ansaldo.it

ABSTRACT

This paper investigates the influence of coolant injection on the aerodynamic and thermal performance of a rotor blade cascade with endwall film cooling. A 7 blade cascade of a high-pressure-rotor stage of a real gas turbine has been tested in a low speed wind tunnel for linear cascades. Coolant is injected through ten cylindrical holes distributed along the blade pressure side. Tests have been preliminarily carried out at low Mach number (Ma_{2is}=0.3). Coolant-to-mainstream mass flow ratio has been varied in a range of values corresponding to inlet blowing ratios M_1 = 0 – 4.0. Secondary flows have been surveyed by traversing a 5-hole miniaturized aerodynamic probe in two downstream planes. Local and overall mixed-out secondary loss coefficient and vorticity distributions have been calculated from measured data. The thermal behaviour has been also analysed by using Thermochromic Liquid Crystals technique, so to obtain film cooling effectiveness distributions. All this information, including overall loss production for variable injection conditions, allow to draw a comprehensive picture of the aero-thermal flow field in the endwall region of a high pressure rotor blade cascade.

NOMENCLATURE

c	blade chord
D	hole diameter
$DR = \rho_c / \rho_\infty$	density ratio
H	blade height
$H_{12} = \delta^*/\theta$	shape factor
L	hole length
$M_1 = \sqrt{\frac{p_{t,c} - p_1}{p_{t,1} - p_1}}$	inlet loss free blowing ratio
Ma	Mach number
$\mathrm{Re}_{2is} = U_{2is} c/\nu$	isentropic outlet Reynolds number
s	blade pitch
T	temperature
Tu	turbulence intensity level
$U = \sqrt{u^2 + v^2 + w^2}$	local mean velocity
u,v,w	streamwise, transverse and spanwise velocity components
X,Y,Z	cascade coordinate system
α	injection angle
β	flow angle (axial direction)
δ	boundary layer thickness
δ^*	displacement thickness
$\eta = (T_{aw} - T_\infty)/(T_c - T_\infty)$	film cooling effectiveness
θ	momentum thickness
ν	kinematic viscosity
ρ	flow density
$\Omega = \Omega_s c/U_1$	non dimensional vorticity
$\zeta = (U_{2is}^2 - U_2^2)/\overline{U}_{2is,ms}^2$	local energy loss coefficient

Subscripts

1	inlet
2	exit
ax	axial
aw	adiabatic wall
c	cooling flow
is	isentropic condition
ms	at mid span
s	streamwise
∞	free stream

Overbar

$\bar{}$	pitch averaged

= mass averaged, area averaged

INTRODUCTION

In modern gas turbines the achievement of high performance requires a continuous increase of turbine inlet temperature. Hence an enhancement of the thermal protection of all the surfaces directly exposed to the hot gases, including endwall regions, is needed.

Many researchers have investigated film cooling on vane endwalls, both through upstream slots [1-3] and discrete holes within the passage [4-11]. From the above studies, it is found that film cooling is strongly affected by endwall secondary flows. The cross flow tends to transport the injected coolant from the pressure side to the suction side of the passage. Previous researches demonstrate that the leading edge region of vane endwall is very difficult to cool using discrete holes. As an alternative to injection from slots, shaped holes for endwall film cooling exhibit a good thermal protection capability as documented by Barigozzi et al. [12,13]. Only a few works in the open literature deal with the film cooling of rotor end walls and blades. Blair [14] deeply analysed the effects of flow three dimensionality on the heat transfer in a rotating blade row. Olson at al. [15] examined the effect of a wake-disturbed flow on heat transfer to a turbine blade. The flow structure in the rotor blade passage has been investigated by Wang et al [16]. Goldstein and Spores [17] detected high heat transfer near the blade-endwall junctions of the passage, due to an intense activity of corner vortices.

A frequent topic in the open literature is the analysis of the film cooling effectiveness due to purging of coolant through a circumferentially arranged slot positioned within the stator-rotor axial gap. The areas that are typically difficult to cool, i.e. the region near the leading edge, can be cooled effectively with the upstream slot injection. Papa et al. [18] performed heat transfer measurements and flow visualizations for different blowing ratios in a linear rotor with an injection slot upstream of rotor blades. Wright et al. [19] documented the detrimental effect of an upstream wake on a film cooled turbine blade platform with stator-rotor purge flow. Pau et al. [20] carried out a complete aero-thermal investigation on the purge and platform film cooling on a transonic turbine stage. Suryanarayanan et al. [21] investigated film cooling through the wheel space cavity in a rotating platform. The coolant ejected from the upstream slot can reduce the secondary flow activity within the passage and can effectively protect regions typically hard to cool.

In some recent works, it has been shown that a complete film cooling protection on a rotating platform can be provided by combining upstream stator-rotor gap ejection and injection from discrete holes located in the rear part of the passage [22-25]. The leading edge region of the platform, which is typically poorly protected by using rows of discrete holes, can be effectively cooled by slot purge flow. Such coolant flow succeeds in cooling the front endwall part, but then it is captured by passage vortex leaving most of the pressure side practically uncooled. The purge flow can be reduced if the rear part of the platform is properly cooled by discrete holes distributed along the pressure side.

The present paper deals with the aerodynamic and thermal behaviour of a rotor blade cascade with a discrete hole cooling scheme on the endwall. The coolant injection holes are located in the rear part of the passage near to the filleted pressure side of the blade, in a region where the thermal protection is usually very critical. The influence of rotor blade fillets on aerodynamic performance of a turbine stage has been numerically investigated in a recent work by Shi et al. [26]. Han and Goldstein [27,28] showed that the fillets can significantly reduce the heat transfer due to the passage vortex (whose strength is typically lowered), but corner vortices near the blade-endwall junction can be intensified and can cause higher heat transfer. The local effectiveness distribution is strongly dependent on the layout: the arrangement of film cooling holes on the platform is a key point. The present cooling scheme was designed with the aim of protect a portion of the endwall exploiting the secondary flow activity within the passage.

EXPERIMENTAL DETAILS

Geometry and test conditions

Tests have been performed at the Turbomachinery Laboratory of the University of Bergamo. It is a continuous running suction type wind tunnel for linear rotor cascades that assures a complete optical access because entirely made up of Plexiglas (Fig. 1).

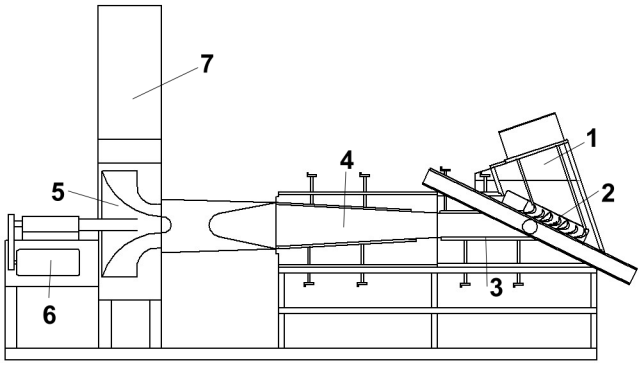

Fig. 1. The wind tunnel (1: inlet duct; 2: test section; 3: tailboard; 4: diffuser; 5: fan; 6: AC motor; 7: discharge channel).

s/c =0.69	H/c = 1.26
c = 116.7 mm	β_2 = -64.19°
β_1 = 44.26°	Ma_{2is} = 0.3
Ma_1 = 0.183	Tu_1 = 1.5 %
Re_{2is} = 0.74 10^6	M_1 = 0 – 3.22

Table 1. Cascade geometry and operating conditions.

The cascade model consists of a 7 blade cascade whose geometry (Fig. 2) is typical of a first high pressure turbine

blade. It has been tested at low Mach number (Ma_{2is}=0.3) with a low inlet turbulence intensity level (Tu_1 = 1.5%). Geometrical details of the cascade and operating conditions are all summarized in Table 1. The inlet boundary layer was investigated by traversing a flattened Pitot tube 0.95 c_{ax} upstream of the leading edge; integral parameters as well as velocity distribution are respectively reported in Table 2 and Fig. 3.

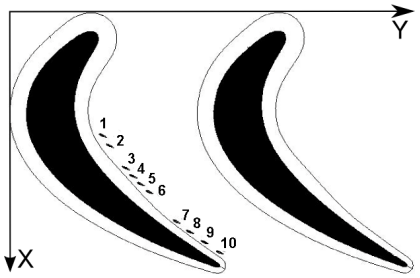

Fig. 2. Cascade and endwall cooling geometry.

δ (mm)	26.4
δ^* (mm)	2.1
H_{12}	1.3

Table 2. Inlet boundary layer integral parameters.

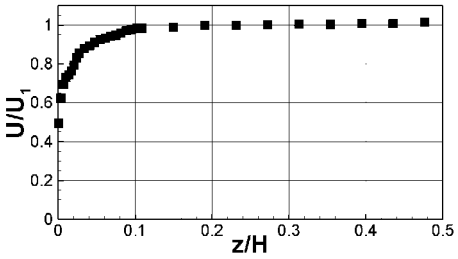

Fig. 3. Inlet velocity profile.

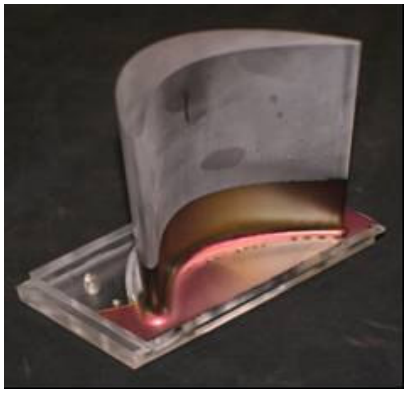

Fig. 4. Cooled blade.

The blade cascade model has been realized in a modular way, allowing to easily change the central passages. Figure 4 shows one of the single blade elements. On the hub side, the connection between the blade and the platform is realized through a 3D fillet, whose trace in the platform plane is depicted in Fig. 2. Please note that only the blade hub to platform junction is filleted.

Only one channel is cooled by means of 10 holes 0.7 mm in diameter, located on the filleted endwall. Within the channel, holes are distributed along the blade pressure side, very close to the fillet region (see Fig. 2 and 4). Positions as well as geometrical details of the cooling apparatus are given in Table 3 and Fig. 5. A unique plenum feeds all the holes (Fig. 6). The plenum is integrated in the blade platform and extends outside of the tunnel. Tests have been carried out for a range of inlet loss free blowing ratios M_1, varying between 0 (no injection) and 4.0.

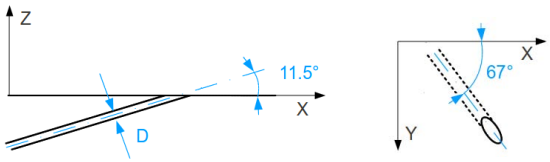

Fig. 5. Detail of holes geometry.

Hole #	*X/c$_{ax}$*	*Y/s*	*L/D*
1	0.440	0.411	20.029
2	0.484	0.446	21.300
3	0.578	0.530	24.329
4	0.612	0.570	25.171
5	0.646	0.611	26.086
6	0.679	0.655	27.114
7	0.804	0.799	36.071
8	0.848	0.871	39.186
9	0.892	0.949	43.243
10	0.935	1.031	48.214

Table 3. Cooling system geometry.

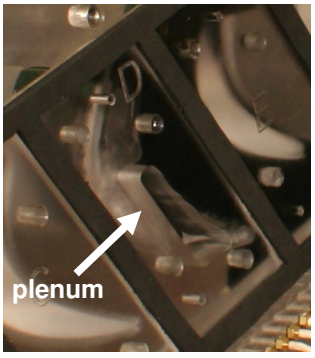

Fig. 6. Detail of coolant supply plenum.

Measurement techniques

Testing conditions were controlled through a continuous monitoring of the coolant total pressure in the feeding chamber. The amount of the injected mass flow was in fact so small to be practically not-measurable with a sufficiently high accuracy. The inlet loss free blowing ratio M_1 was thus used to identify

each injection condition. It is computed through the cascade inlet total (Pitot probe) and static pressures and the coolant total pressure. Coolant total pressure and temperature are measured by a pressure tap and a T-type thermocouple located on the back side wall of the plenum. A HP 3852A D.A.C.U. unit (12 bit resolution) was used to acquire all pressure (± 100 mV range) and temperature data. The uncertainty in the M_1 value was computed on the basis of pressure transducers (± 5.5 Pa) and Pitot probe (± 10 Pa) uncertainties. δM_1 resulted to be ± 0.032 at a value of $M_1 = 0.8$ and ± 0.16 at a value of $M_1 = 4.0$.

Aerodynamic measurements were performed at two locations downstream of the trailing edge plane by using a 5-hole miniaturized aerodynamic pressure probe (1.6 mm head, advanced 50 mm to the stem): 8% and 30% of the axial chord (X/c_{ax} = 108% and 130%). The measurement plane covers two blade passages and extends over the blade span. The measurement grid is made of 30 points per pitch in tangential direction times a maximum of 59 points along the blade height. The grid spacing was reduced approaching the endwall surface: the first measurement point was 1.4 mm far from the wall. The probe was calibrated over a wide range of yaw and pitch angles. Calibration was performed for a Mach number range extending from 0.05 up to 0.6. Uncertainties in both static and total pressures have been estimated to be ±0.15% of dynamic pressure. Cascade inlet total pressure and 5-hole probe data were used to compute kinetic energy loss coefficient ζ, vorticity Ω and deviation angle $\Delta\beta$. In particular, U_{2is} was computed assuming an isentropic expansion from inlet cascade total pressure to exit (X/c_{ax} = 0.08 or 0.30) static pressure. The computed uncertainty in the ζ value was ± 0.3% at ζ = 3% and ± 0.2% at ζ = 30%, while in the flow angle it was ± 1°. Finally, the streamwise vorticity Ω_s was evaluated from Ω_x and Ω_y. While the experimental results allow a direct estimate of Ω_x, Ω_y was computed in an indirect way, by following the procedure suggested by Gregory-Smith et al. [29], based on Crocco relation:

$$\Omega_y = \frac{1}{u}\left(\Omega_x v + \frac{a^2}{\gamma}\frac{\partial \ln p_t}{\partial Z}\right) \qquad (1)$$

A 2D LDV system was used to measure the blade loading (at mid span, 3 mm from blade surface) and the main stream velocity at holes exits (5 mm far from the endwall) in the solid configuration. The light source was a 300 mW Ar+ laser and the measurement volume was 0.11 mm in diameter and 2.38 mm in length. All measurements were carried out acquiring 20000 burst signals at each location. Sawdust smoke was used to seed the flow. The high number of acquired signals assured statistically accurate averages: based on a 95% confidence level, an uncertainty lower than ±0.1% for the mean velocity has been obtained for a turbulence intensity level of 3%.

Sprayable wide banded Thermochromic Liquid Crystals (Hallcrest BM/R25C10WC17-10) were used to get the film cooling effectiveness distributions. TLC images were acquired by using a CCD camera, with a 767x573 pixels resolution. The primary lighting system consists of two 150 W white light sources, each one connected to two optical fibers. The TLC calibration was performed in situ, substituting the blade central passage with a flat aluminium plate. All calibrations and measurements were performed in the dark, in order to eliminate any influence of background illumination. Moreover, an illumination intensity as uniform as possible was provided to the model surface by properly orienting the lighting system, in the meanwhile avoiding any light reflection onto the CCD camera. A temperature gradient along the calibration plate was then generated by placing an electrical resistance on one side and a water cooled channel on the opposite side of the calibration device. This temperature gradient was captured by means of 10 T-type thermocouples installed just underneath the model surface.

During tests the heated flow (DR = 0.95) was suddenly injected into the main flow at ambient temperature. The time history of the TLC image was recorded by the CCD camera, together with the temperature variation inside the feeding chamber T_c and the main flow temperature T_∞. The RGB to hue conversion [30] was applied to the image data recorded after a time period of about 60 s, i.e. when a stable temperature level inside the plenum was reached, as well as on the endwall surface. Each image was selected in such a way to avoid important conduction phenomena in the most critical region, i.e. just upstream of hole locations (see Fig. 2). The time at which thermal conduction reached the external surface was in fact clearly detectable by looking at the recorded images. Please note that this instant always occurred after a stable temperature level inside the plenum was reached.

η computation was based on the stable coolant temperature value reached inside the supply plenum after the selected test time duration and on main stream temperature measured at cascade inlet. The relatively large thickness of the endwall (Plexiglas made) assured to comply with wall adiabatic condition during test duration as well as with the heat conduction through a semi-infinite solid approach.

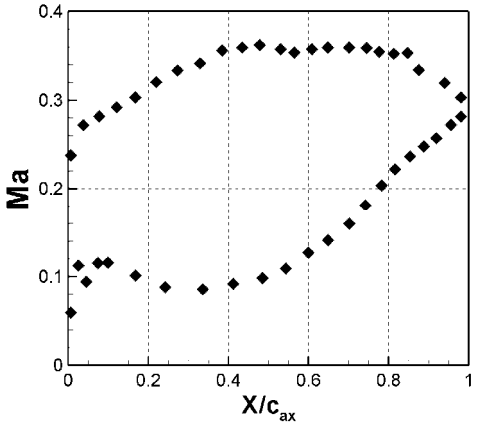

Fig. 7. Blade Mach number distribution.

The film cooling effectiveness measurement uncertainty depends on TLC and thermocouple measurements and

conduction effects. In regions where conduction phenomena do not exist, the η uncertainty will range from ± 5 % with $\eta = 0.5$, up to about ± 15 % when $\eta = 0.1$. Larger uncertainty will exist if conduction phenomena become relevant.

AERODYNAMIC RESULTS

Uncooled blade cascade

The airfoil load measurements (Fig. 7) were performed by LDV at the mid span section of the blade. The flow strongly accelerates around the thin leading edge; on the pressure side a low velocity region extending up to $0.5c_{ax}$ is followed by a continuous acceleration up to the trailing edge. On the suction side, the initial acceleration is followed by a region of approximately constant velocity extending up to about $0.8c_{ax}$, and finally by a moderate diffusion up to the trailing edge. No evidence of flow separation in the pressure side of the leading edge was observed.

Aerodynamic results have been obtained by 5-hole probe traversing in two planes located respectively 0.08 and $0.3c_{ax}$ downstream of the blade trailing edge. The energy loss coefficient ζ contour plots for the uncooled (solid) endwall are shown in Fig. 8, while Fig.9 reports the corresponding vorticity distributions with superimposed secondary velocity vectors.

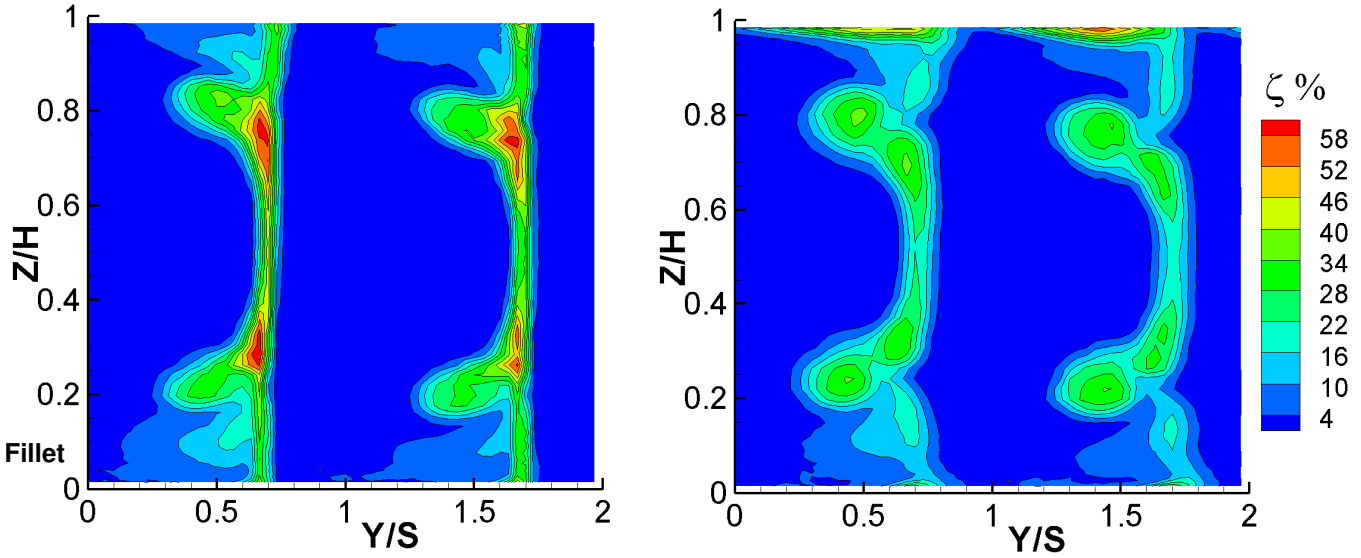

Fig. 8. Solid cascade local ζ distributions: a) X/c_{ax} = 108% and b) X/c_{ax} = 130%.

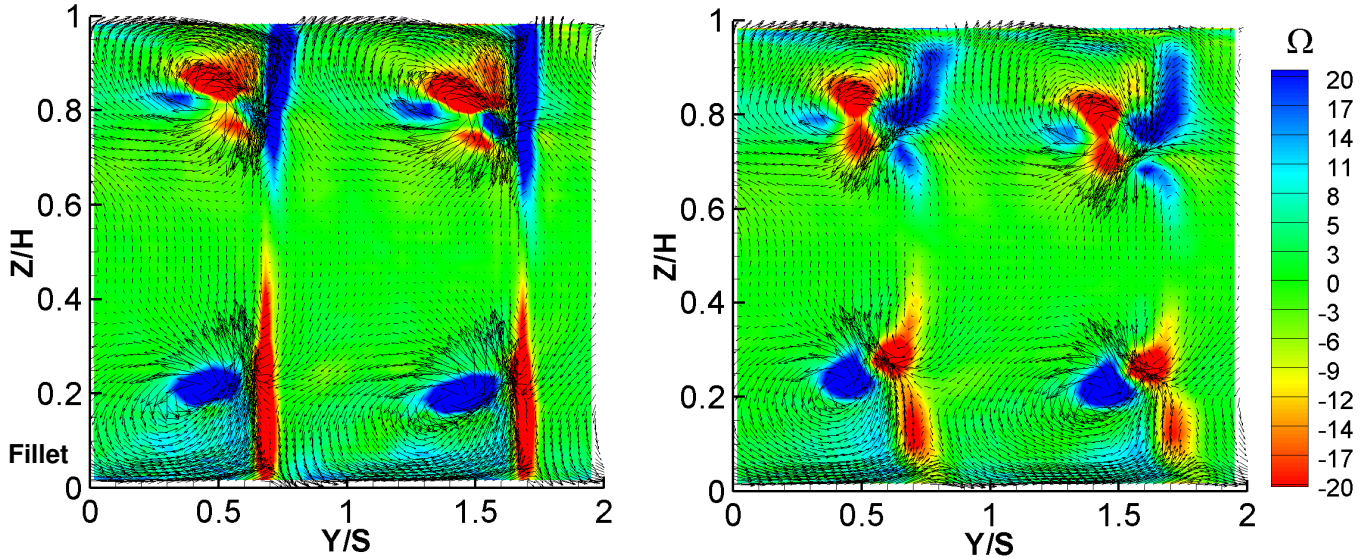

Fig. 9. Solid cascade local Ω and secondary velocity vectors distributions: a) X/c_{ax} = 108% and b) X/c_{ax} = 130%.

Vorticity data are normalized using the blade chord and the cascade inlet velocity U_1. These data represent the reference case for the following cooled endwall investigation; they also allow to analyze the effects of the presence of a 3D fillet at the junction between endwall and blade, as a fillet only exists on the hub side.

Loss coefficient and vorticity distributions both show typical and very well defined secondary flows structures close to cascade exit (Fig. 8a and 9a). The flow field is dominated by the presence of the passage vortex, corresponding to the positive vorticity region (negative vorticity region when looking to the tip side) and to the loss core on the suction side of the blade wake. The high flow turning ($\Delta\beta = 108.45°$) makes the passage vortex position to be significantly shifted towards mid span. This trend continues also after the trailing edge, as can be noted by looking to loss core positions in the two measuring planes. A significant cross flow can be observed in the endwall regions. No trace of corner vortex loss peak can be observed, neither at the hub nor at the tip, probably because it is confined in a thin layer outside of the measuring domain. A very thin wake with a reduced 2D span wise extension can be observed. Looking in more details to the vorticity and secondary velocity vector plots, one can observe a highly three dimensional flow in the plane just downstream of the trailing edge. Besides the passage and the evident trailing shed vorticity, one can identify the suction side leg of the horseshoe vortex between the passage vortex and the trailing shed vorticity region, but this only on the tip side. In fact, at the filleted hub side, besides the trailing shed vorticity, a unique high vorticity core does exist. It means that, at the leading edge, due to the fillet, the intensity of the suction side leg of the horseshoe vortex is so reduced to dissipate before reaching the trailing edge. This even if losses still show a double peak distribution on the wake suction side, usually related to the presence of the suction side horseshoe vortex. Finally, a certain asymmetry in the span wise loss and vorticity distributions can be observed with respect to mid span: all peak values appear to be farer from the wall on the hub side when compared to the tip side. This can be again related to the presence of a fillet that at the leading edge presents a quite relevant span wise extension (5.4%).

Going further downstream (Fig. 8b and 9b) the mixing process goes on: all loss peaks are decreasing, while the regions interested by losses widen. This is the result of secondary velocities and related kinetic energy dissipation that are going to generate secondary loss increase. Still intense vortical structures can be observed, with the trailing shed vorticity that is somewhat distorted, especially at the tip. Here a loss core appears close to the endwall, related to the corner vortex. Surprisingly, in the hub region this loss core is much strongly reduced as clearly indicated both by loss and vorticity distributions. This result disagrees with literature data [27,28,31-32], where the presence of a fillet usually reduces the passage vortex intensity and increases the corner vortex one. A possible reason is the quite big fillet radius at the blade leading edge (see Fig. 2), but it has to be further investigated.

The presented data were obtained at an isentropic downstream Mach number of 0.3. It has to be pointed out that the design operating condition is $M_{2is} = 0.7$. Therefore, at real operating condition some differences are expected to occur. As shown by Perdichizzi [33], secondary flows are expected to be less intense and more confined to the wall region; in particular the endwall cross flow and the related overturning angle would be reduced. This will somewhat modify the coolant to secondary flows interaction, as the injected coolant will better resist to the endwall cross flow.

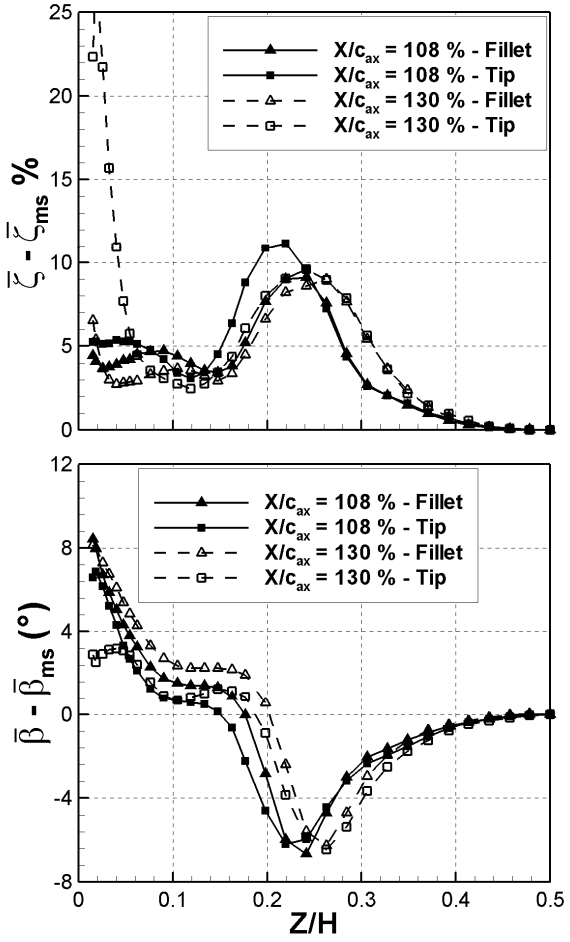

Fig. 10. Spanwise a) primary loss distributions and b) flow angle deviation – no coolant flow.

Starting from flow field measurements in the traversing planes, data were mass averaged (in the tangential direction) over the pitch, to obtain the span wise distributions of loss coefficient and deviation angle reported in Fig. 10. Both solid cascade loss and deviation angle show the typical distribution related to secondary flows. Close to the trailing edge (X/c_{ax} = 108 % - filled symbols), according with Han and Goldstein [27,28], slightly reduced passage and corner vortex related peak loss values take place at the hub, both located farther from the

wall. It has to be pointed out that this is related to the adoption of the fillet that leads to lower losses in the hub region. Going downstream (X/c_{ax} = 130 % - open symbols), due to the mixing, the loss span wise distribution tends to a more uniform and symmetrical pattern, except close to the tip endwall surface, where a strong increase of losses takes place due to the growth of corner vortex loss core gaining in span wise extension.

Comparing hub and tip secondary flow deviation angle distributions, an almost symmetrical distribution takes place close to the trailing edge, with similar peaks of underturning angle (about -6°) and only a slightly reduced overturning at the wall on the tip (7° against 8° on the filleted hub side). Going downstream an overturning decrease down to about 3° on the tip side takes place because of the more intense corner vortex. As a conclusion the adoption of a 3D fillet gives a beneficial effect on endwall losses as reduces the corner vortex intensity, but causes a larger overturning.

Starting from the local flow field measurements (X/c_{ax} = 130%), data were mass averaged over the pitch and over the span to get the overall "primary" loss coefficient:

	ζ (%)
Profile	2.31
Secondary – hub (filleted) side	2.42
Secondary – tip side	3.46
Secondary – full span	2.94
Overall	5.04

Table 4. Solid blade cascade performance.

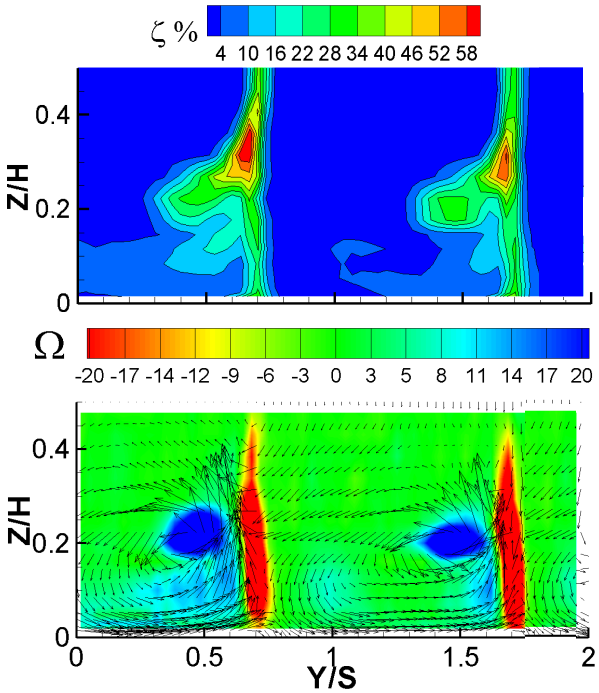

Fig. 11. Cooled cascade local (a) ζ and (b) Ω and secondary velocity vectors distributions at X/c_{ax} = 108% and M_1 = 1.61.

$$\overline{\overline{\zeta}} = \frac{\overline{\overline{U}}_{2is}^2 - \overline{\overline{U}}_2^2}{\overline{U}_{2is,ms}^2} \qquad (2)$$

This formulation does not take into account for the energy related to the coolant flow but, being the injected coolant flow very small compared to the main flow mass flow, it is author's opinion that primary and thermodynamic loss formulation will practically coincide. The secondary loss is obtained by subtracting the pitch wise averaged loss at mid span from the overall loss. Finally, inlet boundary layer loss (1.45 %) has been subtracted from secondary losses. Table 4 summarizes the computed mass averaged profile, secondary and overall kinetic energy loss coefficients. Note that mass averaging was performed twice: from mid span to the hub filleted side and from mid span to the tip side. The thin trailing edge allows a limited profile loss of about 2.3%, while the main contribution to loss generation comes from secondary flows (58%). Tip side secondary flows are responsible for a 3.5% loss production while the filleted hub side contribution is significantly reduced down to about 2.4%.

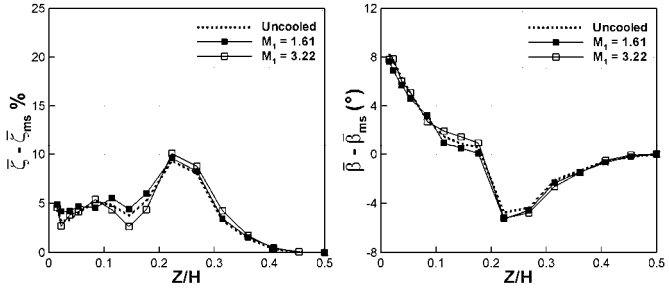

Fig. 12. Spanwise a) flow angle deviation and b) primary loss distributions – with coolant flow.

Cooled blade cascade

A similar investigation was performed on the cooled endwall cascade configuration for variable injection conditions. Figure 11 shows the kinetic energy loss coefficient and the vorticity distributions with superimposed the secondary velocity vectors measured 8% of the axial chord downstream of blade trailing edge. Only data belonging to the injection condition corresponding to an inlet loss free blowing ratio M_1 = 1.61 are here reported and discussed as no significant differences with variable injection conditions were observed.

By comparing Fig. 11 data against the solid (uncooled) results of Fig. 8a and 9a it can be concluded that coolant injection does not significantly alter the flow field: no variations in the secondary flows structure neither in the loss peak levels. This is confirmed by span wise distributions of pitch averaged loss coefficient and deviation angle for two selected injection conditions (M_1 = 1.61 and 3.22) reported in Fig. 12.

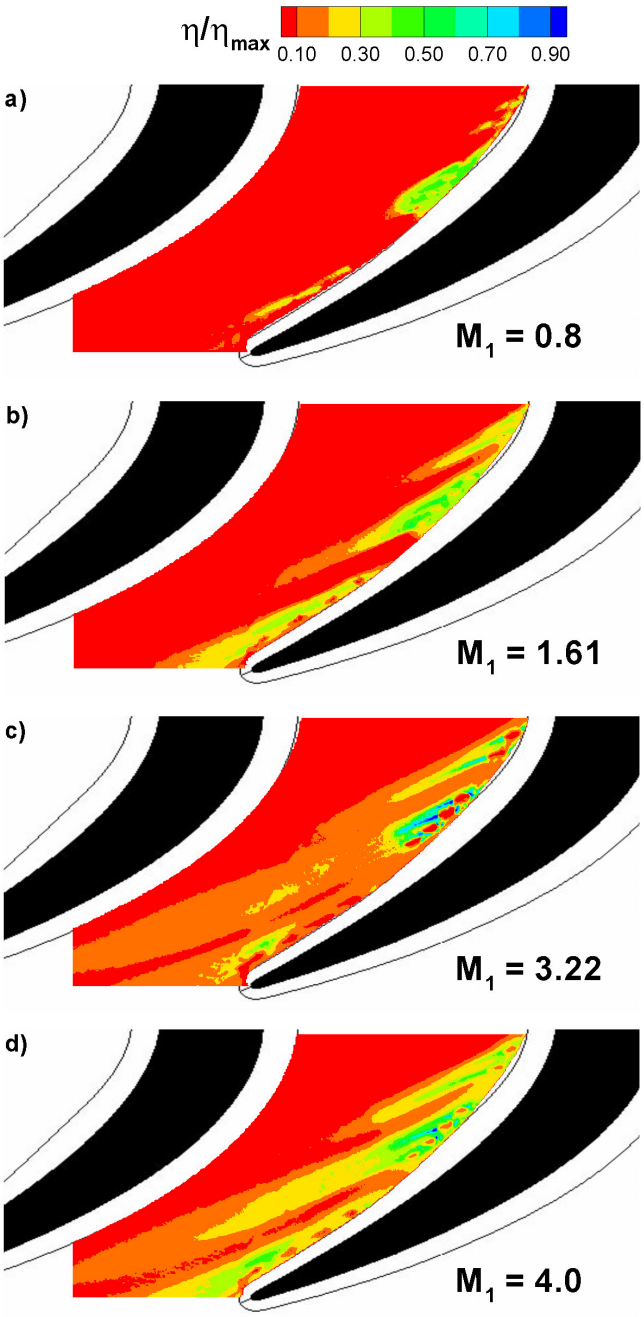

Fig. 13. Film cooling effectiveness distributions for the different injection conditions.

FILM COOLING EFFECTIVENESS RESULTS

To characterize the thermal performance, film cooling effectiveness distributions have been measured at different blowing conditions, ranging from M_1 = 0.8 up to about 4.0. Note that at the lowest injection condition the coolant total pressure established inside the blade cavity is not large enough to ensure a correct coolant ejection from the first two holes. In the largest injection condition holes are not yet chocked: hole #10 isentropic exit Mach number, estimated on the basis of hole exit static pressure (from cascade inlet total pressure and main stream local velocity close to hole exit through LDV measurements) and coolant supply total pressure (measured inside the blade cavity), was about 0.74.

Figure 13 reports the local film cooling effectiveness data for different injection conditions normalized using the maximum detected value η_{max}. As clearly shown, a poor thermal coverage is attained when coolant is injected with low momentum (Fig. 13a - M_1 = 0.8). An insufficient amount of coolant is discharged both through the first 2 holes and through the others located downstream. The area interested by the film cooling is quite limited as coolant quickly mixes with the main flow. Increasing the injection rate to M_1 = 1.61 (Fig. 13b) jet persistency improves downstream of all the holes, but traces belonging to the three sets of holes do not merge. Therefore, most of the endwall remains uncooled. Increasing M_1 up to 3.22 (Fig. 13c) jet persistency improves, even if a quick decay still can be observed downstream of the second group of holes; jet liftoff takes place downstream of the last four holes. However, the whole endwall surface inside the triangle that can be drawn including hole #1 and the trailing edges of the two blades results to be well cooled.

Increasing the inlet blowing ratio even more (Fig. 13e - M_1 = 4.0) film cooling provides a further improvement in the endwall thermal protection, leading to large η values even in the middle of the passage. Probably even better results would be obtained moving the last hole belonging to the second group a little bit downstream. But it has to be observed that, due to the quite low hole injection angle (always about 11°), jet traces still persist significantly, notwithstanding the high jet momentum. Another interesting feature is the fact that jet traces at low injection rates seem not to be strongly affected by secondary flows. This because coolant injection is likely to be performed downstream of the passage vortex separation line, hence the injected flow is not captured by passage vortex and it is only subjected to a moderate endwall cross flow from pressure to suction side. When the jet momentum is increased, jet traces seem to almost maintain the original hole compound angle.

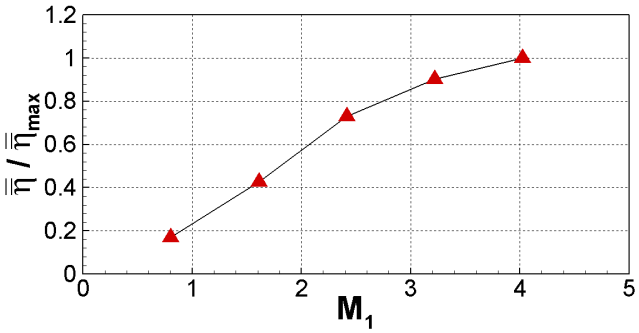

Fig. 14. Area averaged η distributions versus M_1.

Starting from the local η distributions, area averaged values were computed over the region depicted in Fig. 13.

Figure 14 compares the averaged film cooling effectiveness distributions for all the tested injection conditions. Data are normalized using the measured highest value. A progressive increase of thermal protection takes place with rising the injected coolant flow. The area averaged value obtained at M_1 = 1.61, that is a typical value for such a kind of application, can be doubled by doubling the inlet loss free blowing ratio or even a higher protection can be reached increasing M_1 further up before holes become choked.

CONCLUSIONS

An experimental investigation on the aero-thermal effects related to the introduction close to the blade pressure side of cylindrical holes for cooling the inner platform region of a high pressure blade endwall has been carried out. From the presented results the following conclusions can be drawn:

- coolant injection has a negligible impact on aerodynamic performance: no significant variations in the secondary flows structure neither in the loss values were detected;
- the presence of a 3D fillet in the hub region is responsible for a reduction of the corner vortex loss core, in spite of an increase of the overturning at the wall: the global effect is beneficial, giving rise to a significant reduction of secondary loss in the filleted hub side;
- the cooling scheme exhibits a moderate thermal protection of the rear part of the rotor passage at low to mean blowing condition, with the region close to the suction side substantially uncooled;
- increasing the coolant flow rate (up to a quite high value of M_1 = 3.22 or even 4.0), an improvement in the endwall thermal protection takes place, even in the middle of the passage;
- the persistency of jet traces at medium to high injection conditions is good: jets appear to be marginally affected by secondary flows and maintain the original hole compound angle.

Film cooling effectiveness results showed that increasing the coolant flow rate, a better thermal protection of the passage is attained, at the expense of an higher coolant total pressure: the use of larger-diameter holes could be a valid alternative solution to provide high coolant flow rates with moderate coolant total pressure.

ACKNOWLEDGMENTS

The authors wish to thank R2 for models manufacturing and Mr. V. Biondi and E. Gatti for the appreciated technical support.

REFERENCES

[1] Blair M.F., 1974, “An Experimental Study of Heat Transfer and Film Cooling on Large-Scale Turbine Endwalls”, *ASME J. of Heat Transfer*, 96, 524-529.

[2] Roy R.P., Squires K.D., Gerendas M., Song S., Howe W.J., Ansari A., 2000, “Flow and Heat Transfer at the Hub Endwall of Inlet Vane Passages – Experiments and Simulations”, ASME Paper 2000-GT-198.

[3] Oke R.A. and Simon T.W., 2002, “Film Cooling Experiments with Flow Introduced upstream of a First Stage Nozzle Guide Vane through Slots of Various Geometries”, ASME Paper 2002-GT-30169.

[4] Oke R.A., Simon T.W., Burd S.W., Vahlberg R., 2000, “Measurements in a Turbine Cascade over a Contoured Endwall: Discrete Hole Injection of Bleed Flow”, ASME Paper 2000-GT-214.

[5] Jabbari M.J., Marston K.C., Eckert E.R.G. Goldstein R.J., 1996, “Film Cooling of the Gas Turbine Endwall by Discrete-Hole Injection”, *ASME J. of Turbomachinery*, 118, 278-284.

[6] Friedrichs S., Hodson H.P., Dawes W.N., 1996, “Distribution of Film-Cooling Effectiveness on a Turbine Endwall Measured with the Ammonia and Diazo Technique”, *ASME J. of Turbomachinery*, 118, 613-621.

[7] Friedrichs S., Hodson H.P., Dawes W.N., 1997, “Aerodynamic Aspects of Endwall Film-Cooling”, *ASME J. of Turbomachinery*, 119, 786-793.

[8] Friedrichs S., Hodson H.P., Dawes W.N., 1999, “The Design of an Improved Endwall Film-Cooling Configuration”, *ASME J. of Turbomachinery*, 121, 772-780.

[9] Kost F. and Nicklas M., 2001, “Film-Cooled Turbine Endwall in a Transonic Flow Field: Part I – Aero-dynamic Measurements”, ASME Paper 2001-GT-0145.

[10] Nicklas M., 2001, “Film-Cooled Turbine Endwall in a Transonic Flow Field: Part II – Heat Transfer and Film-Cooling Effectiveness”, ASME Paper 2001-GT-0146.

[11] Knost D.G. and Thole K.A., 2004, “Adiabatic Effectiveness Measurements of Endwall Film-Cooling for a First Stage Vane”, ASME Paper 2004-GT-53326.

[12] Barigozzi G., Benzoni G., Franchini G., and Perdichizzi A., 2006, “Fan-shaped Hole Effects on the Aero-Thermal Performance of a Film Cooled Endwall”, *ASME J. of Turbomachinery*, 128, 43-52.

[13] Barigozzi G., Franchini G., Perdichizzi A., 2007, “Endwall Film Cooling through Fan-Shaped Holes with Different Area Ratios,” *ASME J. of Turbomachinery*, 129, 212-220.

[14] Blair M.F., 1994, “An Experimental Study of Heat Transfer in a Large-Scale Turbine Rotor Passage”, *ASME J. of Turbomachinery*, 116, 1-13.

[15] Olson S.J., Sanitjai S., Ghosh K., Goldstein R.J., 2009, “Effect of Wake-Disturbed Flow on Heat (Mass) Transfer to a Turbine Blade”, ASME Paper 2009-GT-60218.

[16] Wang H.-P., Olson S.J., Goldstein R.J. and Eckert E.R.G., 1997. “Flow Visualization in a Linear Turbine Cascade of High Performance Turbine Blades”, *ASME J. of Turbomachinery*, 119, 1-8.

[17] Goldstein R.J. and Spores R.A., 1988, “Turbulent Transport on the Endwall in the Region Between Adjacent Turbine Blades”, *ASME J. of Heat Transfer*, 110, 862-869.

[18] Papa M., Srinivasan V., Goldstein R.J., 2010, "Film Cooling Effect of Rotor-Stator Purge Flow on Endwall Heat/Mass Transfer", ASME Paper 2010-GT-23178.
[19] Wright L.M., Blake S.A., Rhee D.H., Han J.C, 2007, "Effect of Upstream Wake With Vortex on Turbine Blade Platform Film Cooling With Simulated Stator-Rotor Purge Flow", ASME Paper 2007-GT-27092.
[20] Pau M., Paniagua G., Delhaye D., de la Loma A., Ginibre P., 2010, "Aerothermal Impact of Stator-Rim Purge Flow and Rotor-Platform Film Cooling on a Transonic Turbine Stage", *ASME J. of Turbomachinery*, 132, 021006.
[21] Suryanarayanan A., Mhetras S.P., Schobeiri M.T., Han J.C., 2009, "Film-Cooling Effectiveness on a Rotating Blade Platform", *ASME J. of Turbomachinery*, 131, 011014.
[22] Wright L.M., Blake S.A., Han J.C, 2008, "Film Cooling Effectiveness Distributions on a Turbine Blade Cascade Platform With Stator-Rotor Purge and Discrete Film Hole Flows", *ASME J. of Turbomachinery*, 130, 031015.
[23] Gao Z., Narzary D., Han J.C., 2008, "Turbine Blade Platform Film Cooling with Typical Stator-Rotor Purge Flow and Discrete-Hole Film Cooling", ASME Paper 2008-GT-50286.
[24] Yang H., Gao Z., Chen H.C., Han J.C., Schobeiri M.T., 2009, "Prediction of Film Cooling and Heat Transfer on a Rotating Blade Platform With Stator-Rotor Purge and Discrete Film-Hole Flows in a 1 1/2 Turbine Stage", *ASME J. of Turbomachinery*, 131, 041003.
[25] Suryanarayanan A., Ozturk B., Schobeiri M.T., Han J.C., 2010, "Film-Cooling Effectiveness on a Rotating Turbine Platform Using Pressure Sensitive Paint Technique", *ASME J. of Turbomachinery*, 132, 041001.
[26] Shi Y., Li J., Feng Z., 2010, "Influence of Rotor Blade Fillets on Aerodynamic Performance of Turbine Stage", ASME Paper 2010-GT-23721.
[27] Han S. and Goldstein R.J., 2006. "Influence of Blade Leading Edge Geometry on Turbine Endwall Heat (Mass) Transfer", *ASME J. of Turbomachinery*, 128, 798-813.
[28] Han S. and Goldstein R.J. 2007. "Heat Transfer Study in a Linear Turbine Cascade Using a Thermal Boundary Layer Measurement Technique", *ASME J. of Heat Transfer*, 129, 1384-1394.
[29] Gregory-Smith D.G., Graves C.P., Walsh J.A., 1988, "Growth of Secondary Losses and Vorticity in an Axial Turbine Cascade", *ASME J. of Turbomachinery*, Vol. 110, 1-8.
[30] Camci C., Kim K., Hippensteele S.A., 1992, "A New Hue Capturing Technique for the Quantitative Interpretation of Liquid Crystal Images Used in Convective Heat Transfer Studies", *ASME J. of Turbomachinery*, V. 114, 765-775.
[31] Zess G.A. and Thole K.A., 2002, "Computational Design and Experimental Evaluation of Using a Leading Edge Fillet on a Gas Turbine Vane", *ASME J. of Turbomachinery*, V. 124, 167-175.
[32] Pieringer P. and Sanz W., 2004, "Influence of the Fillet between Blade and Casing on the Aerodynamic Performance of a Transonic Turbine Vane", ASME Paper GT2004-53119.
[33] Perdichizzi A., 1990, "Mach Number Effects on Secondary Flow Development Downstream of Turbine Cascade", *ASME J. of Turbomachinery*, V. 112, 643-651.